2019-05-30

Slow light with interleaved p-n junction to enhance performance of integrated Mach-Zehnder silicon modulators

Marco Passoni

Dario Gerace

Liam O'Faolain

Lucio Claudio Andreani

Research article

Marco Passoni, Dario Gerace, Liam O'Faolain and Lucio Claudio Andreani*

Slow light with interleaved p-n junction to enhance performance of integrated Mach-Zehnder silicon modulators

https://doi.org/10.1515/nanoph-2019-0045
Received February 15, 2019; revised April 12, 2019; accepted April 13, 2019

Abstract: Slow light is a very important concept in nanophotonics, especially in the context of photonic crystals. In this work, we apply our previous design of band-edge slow light in silicon waveguide gratings [M. Passoni et al, Opt. Express 26, 8470 (2018)] to Mach-Zehnder modulators based on the plasma dispersion effect. The key idea is to employ an interleaved p-n junction with the same periodicity as the grating, in order to achieve optimal matching between the electromagnetic field profile and the depletion regions of the p-n junction. The resulting modulation efficiency is strongly improved as compared to common modulators based on normal rib waveguides, even in a bandwidth of 20–30 nm near the band edge, while the total insertion loss due to free carriers is not increased. The present concept is promising in view of realizing slow-light modulators for silicon photonics with reduced energy dissipation.

Keywords: silicon photonics; optical modulators; slow light.

1 Introduction

Slowing down the propagation of light waves has been a vibrant area of research in recent years [1]. The speed of light can be reduced to values as low as 17 m/s in ultracold atomic gases by the mechanism of electromagnetically induced transparency [2]. Slow light in photonic integrated circuits, especially in silicon photonics, is much less spectacular in terms of slowdown factors, but potentially more interesting for applications due to the enhancement of light-matter interaction. Key issues for practical applications are the group index enhancement, its tradeoff with the bandwidth, and the propagation losses. Much research and efforts have been devoted to the realization of slow light in two-dimensional (2D) photonic crystal slab waveguides [3, 4]. Indeed, photonic crystals (PhCs) possess many degrees of freedom that can be usefully exploited to realize, e.g. flat-band slow light with designed bandwidth and low group-velocity dispersion [5–8] or the enhancement of nonlinear effects [9–11]. Nevertheless, photonic crystal waveguides require advanced fabrication and are not employed in industrial devices, which are typically based on conventional silicon ridge/rib waveguides.

Our focus here is the application of slow light to integrated Mach-Zehnder (MZ) modulators in the Silicon-On-Insulator (SOI) platform. MZ modulators for silicon photonics are optical modulators that exploit the variation of the refractive index in one or both arms of a MZ interferometer [12–16]. Optical modulators are crucial components for optical communication as they are the active elements that encode the information of a bit stream into the optical carrier wave. For high-speed operation required for optical communication, the most appropriate modulation mechanism exploits the plasma dispersion effect in a reverse-biased p-n junction, namely the change of the refractive index due to a variation of the free-carrier concentration [17]. Standard MZ modulators have two arms made of rib waveguides, which include sections with a lateral p-n junction that act as on optical phase-shifter [18, 19]. The main limitation of such a device is the poor overlap between the depletion region of the p-n junction and the optical mode profile. As the resulting change of the effective refractive index is quite small, the modulator length has to be of the order of millimeters, which in turn determines the capacitance and the power dissipation of the device.

***Corresponding author: Lucio Claudio Andreani,** Department of Physics, University of Pavia, 27100 Pavia, Italy; and CNR-IFN, 20133 Milano, Italy, e-mail: lucio.andreani@unipv.it. https://orcid.org/0000-0003-4926-1749
Marco Passoni and Dario Gerace: Department of Physics, University of Pavia, 27100 Pavia, Italy
Liam O'Faolain: Centre for Advanced Photonics and Process Analysis, Cork Institute of Technology, Cork, Ireland

In our previous work [20] we optimized the geometry for slow light in waveguide gratings (also known as corrugated or fishbone waveguides) that are made of alternating wide/narrow sections of a rib waveguide in SOI. Waveguide gratings are periodic structures along the direction of propagation that lead to photonic stop bands and to slow light close to the band edges. Such waveguide gratings can be incorporated in standard silicon photonic circuits, as they can be connected with silicon rib waveguides by means of low-loss tapers [21–26]. In Ref. [20] we designed the optimized parameters of SOI waveguide gratings for a target wavelength in the O-band ($\lambda = 1.3$ μm) by finding a proper tradoff between the group index enhancement and the slow-light bandwidth. In the present work we optimize phase shifter arms of MZ modulators by matching the optical profile of the slow-light mode with the electrical profile of the free carriers in the p-n junction. This is achieved by using an interleaved p-n junction, which varies periodically along the propagation direction of the optical wave. While previous studies of MZ modulators with either slow light [27–29] or with interleaved p-n junctions [30–33] have been reported, the focus here is the synergic use of both concepts. The combination of slow light and interleaved p-n junction is shown here to yield a modulation efficiency that is considerably improved with respect to standard modulators or to the use of both effects alone, while retaining a wide bandwidth that is essential for optical communication. The designed structure fulfills the required constraints for fabrication on industrial technology platforms [34], and may be suitable for the realization of MZ modulators with reduced energy dissipation.

Despite considerable literature on slow light in 2D photonic crystal waveguides, as discussed above, applications of such slow-light structures to electro-optical modulators are uncommon. A review on slow-light MZ modulators based on Si photonic crystals is given in Ref. [35]. We should notice that slow-light MZ modulators with interleaved (or, more generally, modulated) p-n junctions have been deeply studied in the context of 2D PhC waveguides for wavelengths in the C-band ($\lambda = 1.55$ μm) [36, 37]. The grating waveguides considered here have the advantage of being more compatible with standard silicon photonic circuits on widespread industrial platforms, especially because the structure is simpler and less demanding in terms of optical design and fabrication, and low-loss tapers with standard rib waveguides are easily available. Resonator-based modulators with interleaved p-i-n junctions leading to matching with optical mode have also been developed [38–40]. Such resonators have typically a small bandwidth, unlike the MZ modulators proposed in this work.

The rest of this paper is organized as follows: in Section 2 we briefly review the optimization of band-edge slow-light structures. In Section 3 we describe the interleaved p-n junction and the corresponding electrical simulations. In Section 4 we present the results of electro-optical simulations, which are applied in Section 5 to calculate the modulation efficiency and the propagation losses of phase shifters. The dynamic behavior is also calculated. Section 6 contains a summary and discussion of the results.

2 Slow light in silicon waveguide gratings

The waveguide gratings considered in this work are displayed in Figure 1, and consist of a silicon rib waveguide with periodically modulated waveguide width embedded in SiO_2. The slow-light behavior arises from the flattening of the band dispersion at the edge of a photonic band gap. These structures were systematically studied in our previous work [20], and two optimized configurations will be analyzed here. The common parameters of both structures are the waveguide thickness $s = 310$ nm, the fill-factor $d_1/a = 0.5$ where $a = d_1 + d_2$ is the period, and the widths W_1 and W_2 that are equal to 100 nm and 800 nm, respectively. The two configurations differ mainly for the silicon thickness in the etched cladding regions, t: the first structure

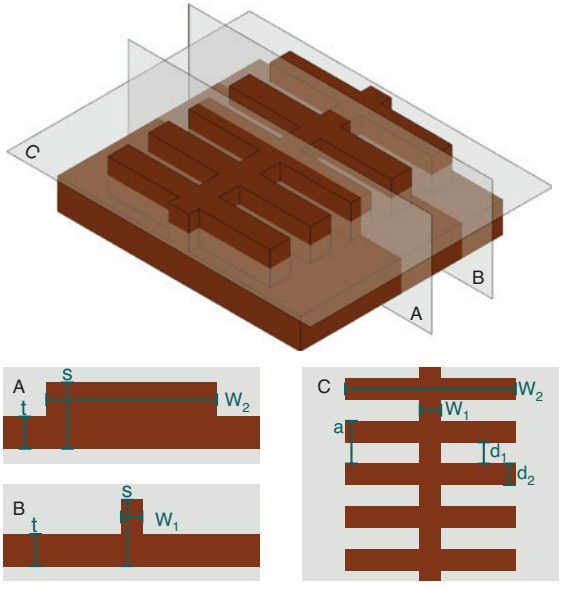

Figure 1: Structure of the slow-light waveguide: 3D view (upper panel) and cross sections (planes A, B, C) with parameters definition. Brown is Si, while the surrounding medium is SiO_2.

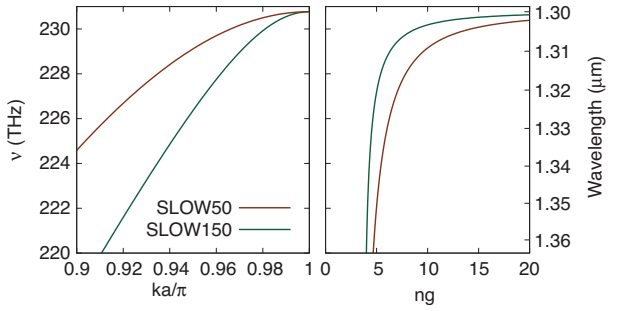

Figure 2: Fundamental band dispersion and group index of the two slow-light configurations adopted in this work.

has $t = 150$ nm and is named SLOW150, while the second structure has $t = 50$ nm and is denoted as SLOW50. These values correspond to common technology platforms for optical interconnects [34]. To lock the lowest band edge at $\lambda = 1.3$ μm, the period has to be fixed as $a = 218.1$ nm and $a = 234.7$ nm for SLOW150 and SLOW50 configurations, respectively.

The photonic band dispersion and group index of the lowest TE mode are plotted in Figure 2 for both SLOW150 and SLOW50 configurations. Both Si and SiO_2 are treated as dispersionless materials with a dielectric constant $\varepsilon = 12.299$ and 2.093, respectively. The increase of the group index in the proximity of the band edge is clearly evident, and it is more prominent in the SLOW50 case, due to the greater strength of the periodic modulation in this configuration. We see, for example, that a group index $n_g > 10$ is compatible with a bandwidth of ~10 nm. Notice that the photonic dispersion lies entirely below the air light line, thus the lowest TE mode is truly guided with no intrinsic losses, while actual propagation losses will be of extrinsic type and related to disorder-induced scattering at the vertical sidewall roughness [41, 42]. The designs fulfill the requirement of a minimum feature size ~100 nm, thus the structures may be fabricated by deep UV lithography with low losses.

3 Electrical structure and simulation

In order to enhance the efficiency of a phase-shifter based on the plasma dispersion effect, it is very important to maximize the overlap between the region in which the refractive index is modified – i.e. the voltage-dependent depletion region of the p-n junction – and the optical mode of the waveguide. In phase shifters based on a conventional rib waveguide, this is usually achieved by using a lateral p-n junction with an optimized junction position [43]. More complex geometries like interleaved [33] or U-shaped [44] p-n junctions have also been considered. In these cases, the geometry of the p-n junction is chosen in order to optimize the overlap with the optical mode in the *transverse* directions, i.e. perpendicular to the waveguide axis.

The scheme proposed in this work consists in an interleaved p-n junction whose period is twice the period of the waveguide grating and with a trench depth W_i of 1 μm, see Figure 3A and B. The goal of such a structure is not only to increase the overlap between the depletion region and the optical mode in the transverse direction, but also to exploit the reshaping of the field profile caused by the slow-light waveguide. Indeed, the electric field – see Figure 3C – has the typical profile of an optical mode near the low energy edge of a band gap, i.e. it is a *dielectric mode* featuring a strong localization of the field in the regions with higher (effective) index, i.e. in the thicker sections of the grating. As a consequence, this particular doping arrangement provides an ideal superposition between the depletion regions of the junction and the dielectric regions in which the electromagnetic field is more intense.

We assume doping concentrations to be $N = 1.4 \times 10^{18}$ cm^{-3} and $P = 5 \times 10^{17}$ cm^{-3} as in the literature [43]. Then, we calculate the charge density in the junction as a function of the applied reverse voltage by employing the software

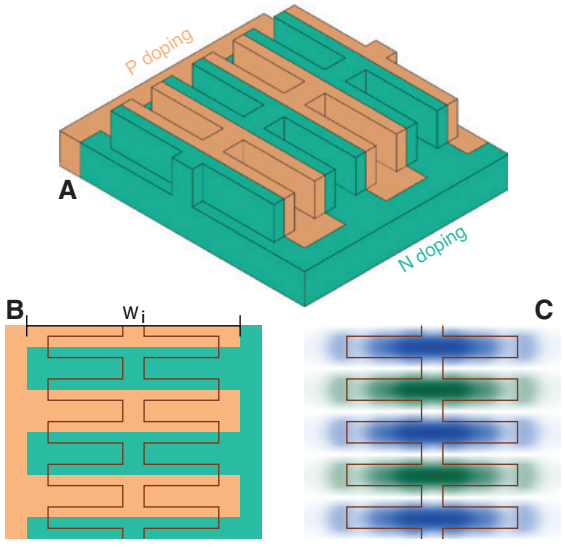

Figure 3: Doping distribution: 3D view (A) and top view (B). In addition, field profile of the optical mode (C) for the SLOW50 waveguide at $\lambda = 1.32$ μm.

Lumerical DEVICE. The code solves the drift-diffusion equations, by applying the finite element method over an unstructured grid [45]. Due to the periodic nature of the structure, the analysis of only one period a is needed, and symmetric boundary conditions are applied along the waveguide direction. The obtained distribution is then interpolated on a regular grid, for clearer visualization and further processing.

As we can see from the example in Figure 4, the depletion region lies in the center of the wider section of the waveguide grating and its width increases with the applied voltage. As a consequence, the refractive index of the waveguide is modified by the plasma dispersion effect. This leads to a phase shift of the propagating optical mode, which is calculated in the next Section. While the charge profiles of Figure 4 are representative of the general behaviour of the interleaved p-n junction in the grating waveguide, the detailed features of the depletion region depend on the exact values of the dopings and also on a possible offset between the junction position and the center of the wide sections. Using a smaller p-type than n-type doping is justified by the fact that the plasma-dispersion effect [Eq. (1) below] is stronger for holes than for electrons. A full optimization of doping levels and profiles has to consider the tradeoffs among various figures of merit (modulator efficiency, losses, cut-off frequency…) and is left for future work. We should also notice that possible deviations or inhomogeneities in doping levels between the unetched and etched regions of the silicon material (as pointed out in Ref. [46]) would not affect the main feature of the present structure, namely the same periodicity of electrical and optical profiles.

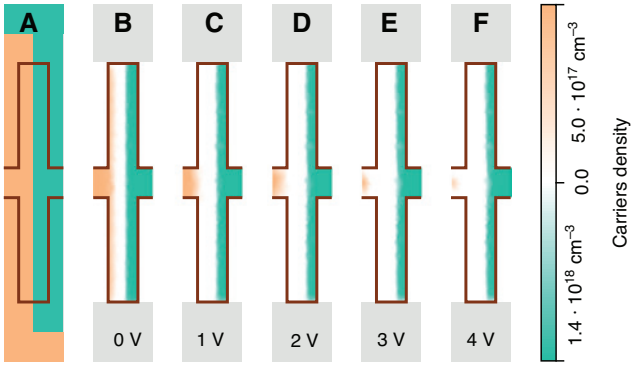

Figure 4: Doping profile within one single period (A) and cross-section of charge distribution as a function of voltage (B–F) for the SLOW50 waveguide. The snapshots are taken at a height of 150 nm from the bottom of the waveguide.

4 Optical simulation

Once the distribution of the free carriers is known, the effect of the applied voltage on the optical mode propagation can be quantified. For this purpose, we first describe the plasma-dispersion effect by converting the charge distribution into a dielectric constant variation using Soref-like equations [17] with textbook coefficients [18]:

$$\Delta n = -3.64 \cdot 10^{-10} \lambda^2 N - 3.51 \cdot 10^{-6} \lambda^2 P^{0.8}, \quad (1)$$

$$\Delta k = 2.80 \cdot 10^{-5} \lambda^3 N + 1.91 \cdot 10^{-5} \lambda^3 P, \quad (2)$$

where N, P are the electrons and holes densities in cm^{-3}, λ is the wavelength in meters (here $\lambda = 1.3$ μm), Δn and Δk are the differences in the real and imaginary part of the refractive index, respectively. The resulting dielectric constant $\varepsilon + \Delta\varepsilon$, where $\Delta\varepsilon = 2\sqrt{\varepsilon}(\Delta n + i\Delta k)$, is plugged into the optical simulation, which then calculates the photonic mode dispersion by the aperiodic Fourier-modal method (A-FMM) [47, 20]. In the process, the dielectric constant in each unit cell is discretized using 40 slices, thus with a spatial resolution of about 5 nm. The required Fourier transforms within a single slice are handled numerically.

In order to describe the performance of the phase shifter in terms of modulation efficiency and propagation losses, we need to calculate the photonic mode dispersion in a periodic grating. In practice, two kinds of optical simulations can be performed. When only the change in the dispersion is needed (i.e. for calculating the phase shift), the optical simulation can be done considering only the change in the real part of the dielectric constant. This greatly simplifies the treatment, since the Bloch vector is purely real and the fitting procedure described in the Appendix can be used. The more complete simulation, including also the imaginary part of the dielectric constant, is used to calculate the propagation loss due to free-carrier absorption, which can be extracted from the imaginary part of the Bloch vector.

In both cases, we need to calculate the scattering matrix for *one period* of the structure. Due to the plasma dispersion effect, the period $2a$ of the waveguide with interleaved doping is twice the period a of the waveguide grating, see Figure 3A and B. However, a simplification can be made by noting that adjacent periods of the waveguide grating, which are different from the electrical point of view, are the mirror image of each other and produce the same phase-shift for the optical mode. We therefore treat two adjacent periods as being identical in the optical simulation, which means that the doped waveguide is still

treated as a periodic medium with period a. This assumption greatly simplifies the calculation, as the resulting band dispersion for the structure with period a can be fitted with an analytic formula with few parameters, as explained in the Appendix. We checked the validity of this approximation by comparing the resulting photonic dispersion with that calculated for the full doped waveguide with period $2a$, finding excellent agreement (deviations on the band dispersion $<10^{-7}$, compared to $\sim 10^{-3}$ variation due to the applied voltage).

The effect of the applied voltage on the band dispersion is displayed in Figure 5 as the difference in the effective (phase) index of the optical modes between the biased and unbiased waveguide. The enhancement due to slow light is evident, as shown by the increase of the effective index difference towards the band edge. As expected, this effect is stronger in the SLOW50 than in the SLOW150 structure, since the SLOW50 structure has an increased slowdown factor that enhances the plasma dispersion effect.

In addition, in Figure 6 we report the excess loss due to free-carrier absorption for both slow-light configurations, extracted from the imaginary part of the effective index of the mode as $\alpha = (20/\ln 10) \cdot \omega k_{\text{eff}}/c$. The plotted results refer to the unbiased waveguides, and represent in a sense the worst-case scenario, since reverse-biasing the junction reduces the absorption loss by lowering the free-carrier density in the waveguide. It can be seen that both configurations exhibit an increased propagation loss towards the band edge, as is well known to happen for slow light. However, the relevant quantity is the total insertion loss of the phase shifter, which is evaluated in the next Section.

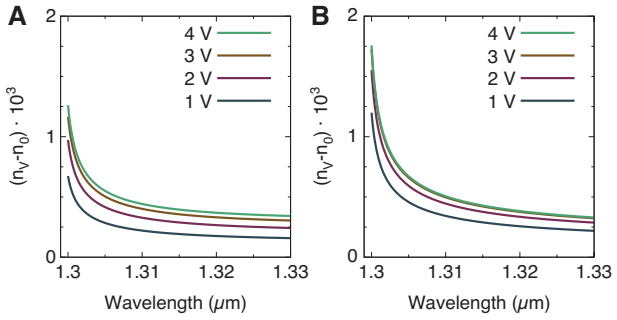

Figure 5: Difference in effective (phase) index between the biased and un-biased waveguides at different values of applied reverse voltage for SLOW150 (A) and SLOW50 (B) configurations.

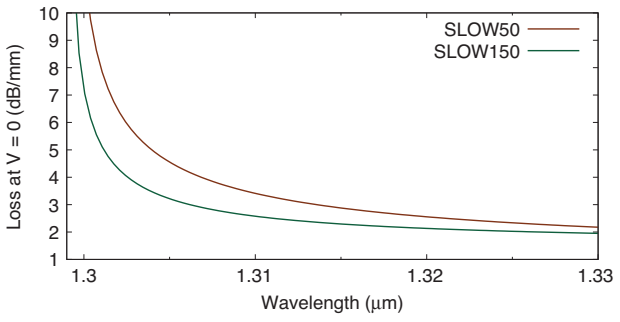

Figure 6: Additional loss due to free-carrier absorption for both SLOW150 and SLOW50 configurations.

5 Results on phase-shifters

The main figure of merit for a phase-shifter is usually taken to be $V_\pi L_\pi$, namely, the product of the driving voltage and of the length that is needed to yield a π phase difference with respect to the unbiased case. $V_\pi L_\pi$ is commonly referred to as the *modulation efficiency*, and it generally increases as a function of the applied reverse voltage V, since the width of the depletion region increases sublinearly with V and so does the phase shift at a fixed length. In general, $V_\pi L_\pi$ depends also on the wavelength, but in phase-shifters based on conventional rib waveguides this dependence is negligible. This is not the case in our slow-light waveguides, because the phase modulation is closely related to the group index, which depends strongly on the wavelength.

As for the insertion loss, a common figure of merit is IL(L_π), obtained as the propagation loss per unit length α times the length L_π. Here, α is calculated at $V=0$, while L_π depends on the voltage: this should again be viewed as a quantification of losses in a worst-case scenario, and it applies to MZ modulators in a push-pull configuration where one of the two phase shifters is always kept at $V=0$ [19]. A typical modulator operates with a phase shift $\sim 0.15\pi$ in each arm, thus the length has to be $L = 0.15 L_\pi$ and the actual insertion loss is $\sim 0.15 \cdot \text{IL}(L_\pi)$.

The obtained $V_\pi L_\pi$ as a function of wavelength is reported in Figure 7 for both SLOW150 and SLOW50 configurations. The effect of slow light is clearly evident, as $V_\pi L_\pi$ decreases monotonically when moving towards the band edge, where the group index increases. Taking advantage of this effect, values of $V_\pi L_\pi$ around 0.1 V cm can be reached, although within a small spectral window (1-2 nm wide) in the proximity of the band edge. This value for the modulation efficiency is about one order of magnitude lower than those obtained in conventional ridge waveguides, where $V_\pi L_\pi$ is typically above 1 V cm [15]. Performance of the slow-light structures remains good even

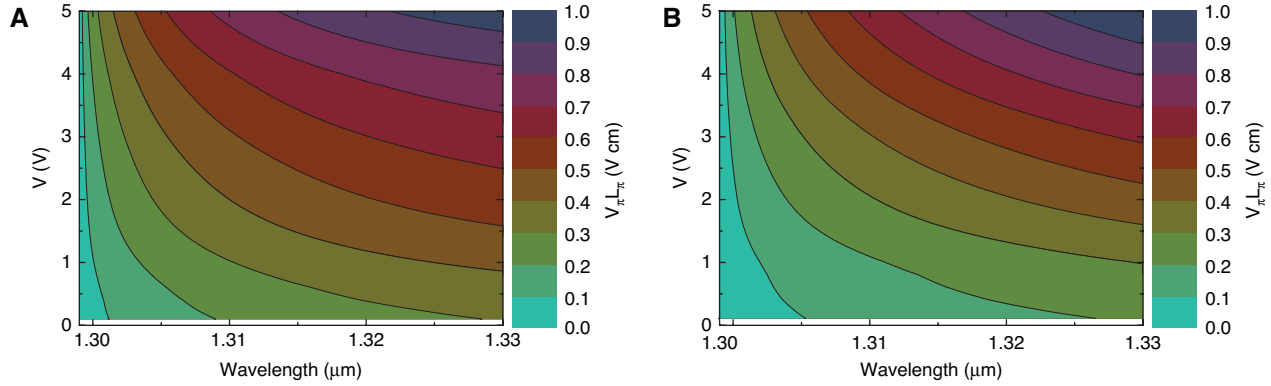

Figure 7: Modulation efficiency as a function of wavelength and applied reverse bias for SLOW150 (A) and SLOW50 (B) configurations.

when a greater bandwidth is required. In particular, the SLOW50 configuration at low voltage shows a $V_\pi L_\pi$ lower than 0.3 V cm over a spectral window of about 30 nm, which is adequate for many telecom applications. This wide bandwidth follows from the spatial matching of the electromagnetic field profile with the depletion region of the p-n junction, which is maintained in a wide spectral region below the band edge.

To see the advantage of the present slow-light design, we present in Table 1 a comparison between the calculated performance of the SLOW50 structure and those of two representative rib waveguides with lateral and interleaved p-n junctions, respectively [33]. Considering first the modulation efficiency $V_\pi L_\pi$, we notice that the interleaved p-n junction gives an improvement over the lateral p-n junction even in a normal rib waveguide configuration [33]. When the slow-light structure is considered, $V_\pi L_\pi$ is further reduced to values as low as 0.1–0.3 V cm at 5–10 nm from the band edge $\lambda = 1.3$ μm. This clearly shows the advantage of combining slow light with the interleaved p-n junction, which strongly improves the performance in a wide bandwidth. Considering now the losses, the propagation loss in dB/cm increases, when going from the normal, to the interleaved, to the slow-light structures: however, IL(L_π) is nearly the same for all configurations. In practice, this means that the optimal length of a slow-light modulator can be a fraction of a mm, i.e. much smaller than in conventional modulators, thus yielding the same total insertion loss but with a strongly improved modulation efficiency.

Reducing the modulator length has also the advantage of improving tolerance against disorder-induced losses due to fabrication processes. A modulator length below 500 μm means that propagation losses up to several 10 dB/cm can be tolerated, which is well within the reach of current fabrication technologies, with margins of improvement thanks to the use of immersion lithography [16].

It is also interesting to quantify the effect of p-n junction geometry in the slow-light structure. For this purpose, we calculate the figures of merit for the SLOW50 configuration but using a lateral p-n junction with the same doping levels. At $\lambda = 1330$, 1320, 1310, 1305 nm and $V = 1$ V we obtain $V_\pi L_\pi = 0.94$, 0.79, 0.59, 0.45 V cm, respectively, which is nearly three times larger than for the interleaved p-n junction. For the same wavelengths, the propagation losses at $V = 0$ are 28.7, 34.0, 45.8, 60.4 dB/cm, leading to IL(L_π) ~27 dB at 1 V, which is much higher than the values reported in Table 1. Thus, we conclude that the use of the interleaved p-n junction greatly improves the efficiency and reduces the insertion loss of the slow-light modulator, thereby demonstrating the key role of spatial matching between the p-n junction and the optical field profile.

Table 1: Modulation efficiency $V_\pi L_\pi$, loss per unit length at $V = 0$, and insertion loss IL(L_π). Both $V_\pi L_\pi$ and IL(L_π) are given for two different values of the applied reverse bias.

Configuration	$V_\pi L_\pi$ (V · cm)		α@0 V (dB/cm)	IL(L_π) (dB)	
	1 V	3 V	–	1 V	3 V
Rib Lateral [33]	1.180	1.500	9.2	10.9	4.60
Rib Interleaved [33]	0.510	0.700	13.5	6.90	3.10
SLOW50@1330 nm	0.304	0.617	21.7	6.60	4.47
SLOW50@1320 nm	0.257	0.526	25.6	6.57	4.49
SLOW50@1310 nm	0.191	0.395	34.2	6.52	4.50
SLOW50@1305 nm	0.143	0.297	45.0	6.42	4.45

Rib lateral (interleaved): normal rib waveguide configuration with lateral (interleaved) p-n junction [33]. SLOW50: slow-light configuration of this work with $t = 50$ nm, at four different wavelengths.

To calculate the frequency response of the phase shifter, we model the structure as an RC circuit and analyse the small-signal response with Lumerical DEVICE. The resistance and the capacitance are obtained from the complex impedance $Z=R+1/(j\omega C)$. The 3 dB cutoff frequency is calculated as $f_{3dB}=1/(2\pi RC)$, and it is independent of the modulator length L, since $C\propto L$ and $R\propto 1/L$. The simulation setup now includes additional highly doped $p+$ and $n+$ regions, see Figure 8A. We choose $W_d=1.2$ µm, a total width $W_t=2.0$ µm, and dopings of 1×10^{19} cm^{-3} in the $p+$ and $n+$ regions, with metal contacts at the borders. With these values the waveguide propagation losses are not increased over those reported in Figure 6, as we have verified. The results as a function of bias voltage are reported in Figure 8. The behavior is similar for the two slow-light configurations, showing an increase of resistance and a decrease of capacitance for increasing voltage, both effects being caused by an expansion of the depletion region. The SLOW50 configuration has higher resistance and lower capacitance compared to the SLOW150 configuration, the first effect dominates and leads to a smaller cut-off frequency. The SLOW150 configuration can reach $f_{3dB}>12.5$ GHz, which can sustain a bit rate up to 25 Gbps with non-return to zero format, or even up to 50 Gbps with PAM-4 encoding [48]. The corresponding rates for the SLOW50 configuration are about a factor of two smaller. There is much room for improving the dynamic behavior by tailoring the doping levels and the spatial profiles of both low- and highly doped regions. Systematic optimization is left for future work.

The advantage of the slow-light modulator design becomes more useful at small driving voltage, which has a beneficial effect on the energy dissipation given by $CV^2/2$. To give an example, we consider both SLOW50 and SLOW150 configurations at 1 V reverse bias. The capacitances per unit length (considering the average values at 0.5 V) are $C/L=1.8$ pF/mm and 2 pF/mm, respectively. Working at $\lambda=1310$ nm, the efficiencies are $V_\pi L_\pi=0.191$ V cm and 0.297 V cm, therefore a phase shift of 0.15π is obtained with length L = 0.15 $L_\pi=290$ µm for SLOW50 and $L=450$ µm for SLOW150 configuration. The energy dissipation is then 0.26 pJ/bit for SLOW50 and 0.45 pJ/bit for SLOW150. These values are reduced up to one order of magnitude compared to typical modulators based on normal rib waveguides [14, 19], and are comparable to those obtained with PhC waveguides [37].

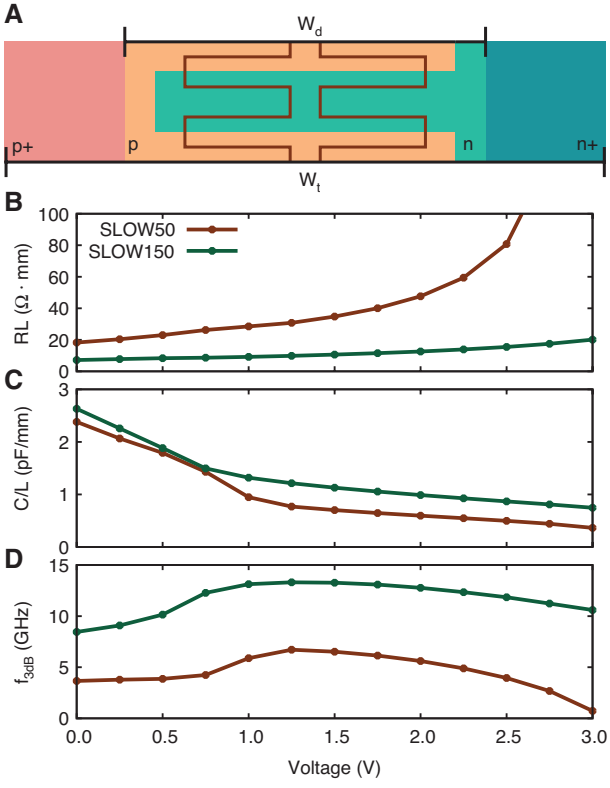

Figure 8: (A) Structure layout for calculating the cutoff frequency, (B) resistance times length, (C) capacitance per unit length, (D) 3-dB cutoff frequency f_{3dB}.

6 Conclusion

Summarizing, we propose a new strategy for exploiting slow light in silicon Mach-Zehnder modulators. The idea is to combine band-edge slow light in a waveguide grating with an interleaved p-n junction along the propagation direction, which has the same period of the optical waveguide. This leads to optimal matching between the propagating electric field and the depletion regions of the p-n junctions, and results in a strongly improved modulation efficiency over a bandwidth up to 20–30 nm. The use of an interleaved p-n junction is especially useful to increase the bandwidth of the slow-light modulator, as the spatial matching between the depletion region and the field profile in the waveguide grating is wavelength-independent. The modulation efficiency $V_\pi L_\pi$ is in the range 0.1–0.5 V cm, depending on the operating bandwidth and on the driving voltage, the best performances being obtained at low voltage $V\sim1$ V.

It is important to notice that the total loss of the slow-light design presented here is not increased with respect to modulators based on normal rib waveguides. Interestingly, the use of an interleaved p-n junction significantly reduces the loss of the slow-light structure relative to a lateral p-n junction: e.g., IL(L_π) ~27 dB and ~6.5 dB with

lateral and interleaved p-n junction, respectively (the corresponding insertion losses for a length $L = 0.15L_{\pi}$ are 4 and 1 dB). In summary, the use of the interleaved p-n junction in the slow-light modulator improves the efficiency and reduces the free-carrier induced insertion losses.

A notable simplification in these time-consuming calculations is given by the procedure that relies on the photonic band structure for a single period, which is fitted with a simple analytic formula. It should be remarked that the present design is not especially optimized. Further improvements of the modulation efficiency are expected by optimizing the doping and/or the junction position inside the waveguide. The present structures can support high-speed modulation, and there is room for improving the cutoff frequency by tuning the doping levels and doping profiles both inside and outside the waveguide. Clearly, a proper tradeoff between modulation rate, losses, and energy consumption will have to be determined for specific applications. Thus, we expect that further improvement of modulator performance will be possible, and that the present concepts can find application to reduce the energy dissipation in MZ modulators on current-day technology platforms.

Appendix

A Phase shift, fitting procedure and parameters

Once the photonic band dispersion in the waveguide grating is calculated, the phase shift of one modulator arm is obtained as $\Delta\phi(\omega) = k(\omega)L$, where $k(\omega)$ is the wavevector as a function of frequency and L is the length of the phase shifter arm. The calculations are greatly simplified by fitting the band dispersion with an analytic formula that results from perturbation theory [20]. The dimensionless frequency $\Omega = \frac{\omega a}{2\pi c}$ is related to the dimensionless distance from the band edge $\delta = \frac{\pi}{a}(1-k)$ using the following formula:

Table 2: Fitting parameters for both slow-light configurations at different voltages.

V (Volts)	SLOW150			SLOW50		
	Ω_0	n	U	Ω_0	n	U
0.0	0.17389030	3.20361349	0.08425434	0.20768102	2.65742768	0.29633870
0.2	0.17388891	3.20364850	0.08426037	0.20767902	2.65745977	0.29634149
0.4	0.17388764	3.20368052	0.08426414	0.20767720	2.65748887	0.29634200
0.6	0.17388647	3.20371049	0.08426610	0.20767547	2.65751647	0.29634115
0.8	0.17388541	3.20373804	0.08426601	0.20767378	2.65754360	0.29633936
1.0	0.17388443	3.20376366	0.08426442	0.20767232	2.65756777	0.29633627
1.2	0.17388351	3.20378778	0.08426174	0.20767116	2.65758705	0.29633271
1.4	0.17388264	3.20381095	0.08425839	0.20767018	2.65760320	0.29632915
1.6	0.17388178	3.20383367	0.08425468	0.20766931	2.65761748	0.29632561
1.8	0.17388094	3.20385606	0.08425068	0.20766847	2.65763124	0.29632202
2.0	0.17388012	3.20387811	0.08424645	0.20766765	2.65764472	0.29631838
2.2	0.17387932	3.20389974	0.08424204	0.20766687	2.65765759	0.29631480
2.4	0.17387854	3.20392084	0.08423749	0.20766617	2.65766940	0.29631141
2.6	0.17387779	3.20394129	0.08423280	0.20766552	2.65768026	0.29630821
2.8	0.17387709	3.20396086	0.08422797	0.20766494	2.65769002	0.29630525
3.0	0.17387643	3.20397924	0.08422308	0.20766447	2.65769813	0.29630274
3.2	0.17387580	3.20399674	0.08421816	0.20766415	2.65770378	0.29630104
3.4	0.17387520	3.20401394	0.08421311	0.20766398	2.65770655	0.29630020
3.6	0.17387461	3.20403074	0.08420800	0.20766396	2.65770686	0.29630011
3.8	0.17387408	3.20404619	0.08420320	0.20766394	2.65770712	0.29630004
4.0	0.17387368	3.20405790	0.08419947	0.20766392	2.65770735	0.29629998
4.2	0.17387355	3.20406141	0.08419834	0.20766390	2.65770757	0.29629993
4.4	0.17387351	3.20406218	0.08419809	0.20766389	2.65770778	0.29629988
4.6	0.17387348	3.20406279	0.08419790	0.20766387	2.65770798	0.29629984
4.8	0.17387345	3.20406328	0.08419775	0.20766385	2.65770817	0.29629980
5.0	0.17387343	3.20406371	0.08419763	0.20766384	2.65770835	0.29629976

Periods are 218.0879 nm and 234.7165 nm for SLOW150 and SLOW50 configurations, respectively.

$$\Omega(\delta)=\left[\Omega_0^2+\frac{\delta^2-\sqrt{4\delta^2+(1-\delta^2)^2U^2}}{4n^2}\right]^{\frac{1}{2}}, \quad (3)$$

which is the corrected form of the one reported in [20]. The fitting parameters Ω_0, n, U represent the midgap frequency, the effective index, and the coupling factor, respectively.

Since the dispersions of the same waveguide at different voltages are quite close to each other, a great precision is needed in the fit. For this reason, in this work the fitting procedure is carried out using up to 100 energy points for each curve. This allows to capture even the small differences in the dispersion as a function of the applied voltage.

Once the fitting parameters and the period are known, it is thus possible to use Eq. (3) to reconstruct the relation between frequency ω and wavevector k. The modulation efficiency is then obtained as $V_\pi L_\pi = V\cdot\pi/\Delta k(\omega)$, where $\Delta k = k_V(\omega) - k_0(\omega)$ is the change in wavevector induced by the plasma dispersion effect. For completeness we report in Table 2, the fitting parameters, as a function of reverse bias, for both SLOW150 and SLOW50 configurations.

Acknowledgments: The authors are grateful to C. Baudot, A. Fincato, A. Ghilioni, R. Sheehan, A. Simbula, F. Svelto, E. Temporiti for many useful discussions and suggestions. We acknowledge the CINECA-ISCRA award for the availability of high performance computing resources and support. This work was supported by the European Union under H2020-ICT27-2015 project no. 688516 COSMICC, Funder Id: http://dx.doi.org/10.13039/100010661, and by EU H2020 QuantERA ERA-NET Co-fund in Quantum Technologies project CUSPIDOR, Funder Id: http://dx.doi.org/10.13039/501100003407, co-funded by Italian MIUR and Science Foundation Ireland under grant 17/QERA/3472.

References

[1] Khurgin JB. Slow light in various media: a tutorial. Adv Opt Photon 2010;2:287–318.
[2] Vestergaard Hau L, Harris SE, Dutton Z, Behroozi CH. Light speed reduction to 17 metres per second in an ultracold atomic gas. Nature 1999;397:594.
[3] Krauss TF. Why do we need slow light? Nat Photon 2008;2:448.
[4] Baba T. Slow light in photonic crystals. Nat Photon 2008;2:465.
[5] Petrov AY, Eich M. Zero dispersion at small group velocities in photonic crystal waveguides. Appl Phys Lett 2004;85:4866–8.
[6] Li J, White TP, O'Faolain L, Gomez-Iglesias A, Krauss TF. Systematic design of flat band slow light in photonic crystal waveguides. Opt Express 2008;16:6227–32.
[7] Hao R, Cassan E, Le Roux X, et al. Improvement of delay-bandwidth product in photonic crystal slow-light waveguides. Opt Express 2010;18:16309–19.
[8] Tamura T, Kondo K, Terada Y, Hinakura Y, Ishikura N, Baba T. Silica-clad silicon photonic crystal waveguides for wideband dispersion-free slow light. J Lightwave Technol 2015;33:3034–40.
[9] Corcoran B, Monat C, Grillet C, et al. Green light emission in silicon through slow-light enhanced third-harmonic generation in photonic-crystal waveguides. Nat Photon 2009;3:206–10.
[10] Monat C, Ebnali-Heidari M, Grillet C, et al. Four-wave mixing in slow light engineered silicon photonic crystal waveguides. Opt Express 2010;18:22915–27.
[11] Matsuda N, Kato T, Harada K, et al. Slow light enhanced optical nonlinearity in a silicon photonic crystal coupled-resonator optical waveguide. Opt Express 2011;19:19861–74.
[12] Reed GT, Mashanovich G, Gardes FY, Thomson DJ. Silicon optical modulators. Nat Photon 2010;4:518.
[13] Miller D. Energy consumption in optical modulators for interconnects. Opt Express 2012;20:A293–308.
[14] Thomson DJ, Gardes FY, Fedeli J-M, et al. 50-Gb/s silicon optical modulator. IEEE Photon Technol Lett 2012;24:234–6.
[15] Reed GT, Mashanovich GZ, Gardes FY, et al. Recent breakthroughs in carrier depletion based silicon optical modulators. Nanophotonics 2013;3:229–45.
[16] Thomson D, Zilkie A, Bowers JE, et al. Roadmap on silicon photonics. J Opt 2016;18:073003.
[17] Soref RA, Bennett BR. Electrooptical effects in silicon. IEEE J Quantum Electron 1987;23:123–9.
[18] Chrostowski L, Hochberg M. Silicon photonics design: from devices to systems. Cambridge, Cambridge University Press, 2015.
[19] Temporiti E, Ghilioni A, Minoia G, et al. Insights into silicon photonics Mach–Zehnder-based optical transmitter architectures. IEEE J Sol State Circuits 2016;51:3178–91.
[20] Passoni M, Gerace D, O'Faolain L, Andreani LC. Optimizing band-edge slow light in silicon-on-insulator waveguide gratings. Opt Express 2018;26:8470–8.
[21] Povinelli ML, Johnson SG, Joannopoulos JD. Slow-light, band-edge waveguides for tunable time delays. Opt Express 2005;13:7145–59.
[22] Cheben P, Bock PJ, Schmid JH, et al. Refractive index engineering with subwavelength gratings for efficient microphotonic couplers and planar waveguide multiplexers. Opt Lett 2010;35:2526–8.
[23] Oskooi A, Mutapcic A, Noda S, Joannopoulos JD, Boyd SP, Johnson SG. Robust optimization of adiabatic tapers for coupling to slow-light photonic-crystal waveguides. Opt Express 2012;20:21558–75.
[24] Bao C, Hou J, Wu H, et al. Flat band slow light with high coupling efficiency in one-dimensional grating waveguides. IEEE Photon Technol Lett 2012;24:7–9.
[25] Cheben P, Schmid JH, Wang S, et al. Broadband polarization independent nanophotonic coupler for silicon waveguides with ultra-high efficiency. Opt Express 2015;23:22553–63.
[26] Sciancalepore C, Hassan K, Ferrotti T, et al. Low-loss adiabatically-tapered high-contrast gratings for slow-wave modulators on SOI. In: High Contrast Metastructures IV, vol. 9372. International Society for Optics and Photonics, 2015, p. 93720G.
[27] Brimont A, Thomson DJ, Gardes FY, et al. High-contrast 40 Gb/s operation of a 500 μm long silicon carrier-depletion slow wave modulator. Opt Lett 2012;37:3504–6.

[28] Brimont A, Gutierrez AM, Aamer M, et al. Slow-light-enhanced silicon optical modulators under low-drive-voltage operation. IEEE Photon J 2012;4:1306–15.
[29] Hosseini R, Mirzoyan L, Jamshidi K. Energy consumption enhancement of reverse-biased silicon-based Mach-Zehnder modulators using corrugated slow light waveguides. IEEE Photon J 2018;10:1–7.
[30] Li Z-Y, Xu D-X, McKinnon WR, et al. Silicon waveguide modulator based on carrier depletion in periodically interleaved pn junctions. Opt Express 2009;17:15947–58.
[31] Yu H, Pantouvaki M, Van Campenhout J, et al. Performance tradeoff between lateral and interdigitated doping patterns for high speed carrier-depletion based silicon modulators. Opt Express 2012;20:12926–38.
[32] Marris-Morini D, Baudot C, Fédéli J-M, et al. Low loss 40 Gbit/s silicon modulator based on interleaved junctions and fabricated on 300 mm SOI wafers. Opt Express 2013;21:22471–5.
[33] Pérez-Galacho D, Marris-Morini D, Stoffer R, et al. Simplified modeling and optimization of silicon modulators based on free-carrier plasma dispersion effect. Opt Express 2016;24:26332–7.
[34] Boeuf F, Crémer S, Temporiti E, et al. Silicon photonics R&D and manufacturing on 300-mm wafer platform. J Lightwave Technol 2016;34:286–95.
[35] Baba T, Nguyen HC, Yazawa N, et al. Slow-light Mach-Zehnder modulators based on Si photonic crystals. Sci Technol Adv Mat 2014;15:024602.
[36] Hinakura Y, Terada Y, Tamura T, Baba T. Wide spectral characteristics of Si photonic crystal Mach-Zehnder modulator fabricated by complementary metal-oxide-semiconductor process. Photonics 2016;3:17.
[37] Terada Y, Tatebe T, Hinakura Y, Baba T. Si photonic crystal slow-light modulators with periodic p–n junctions. J Lightwave Technol 2017;35:1684–92.
[38] Al-Saadi A, Eichler HJ, Meister S. High speed silicon electro-optic modulator with p-i-n comb diode. Opt Quantum Electron 2012;44:125–31.
[39] Meister S, Rhee H, Al-Saadi A, et al. Matching p-i-n-junctions and optical modes enables fast and ultra-small silicon modulators. Opt Express 2013;21:16210–21.
[40] Kupijai S, Rhee H, Al-Saadi A, et al. 25 Gb/s silicon photonics interconnect using a transmitter based on a node-matched-diode modulator. J Lightwave Technol 2016;34:2920–3.
[41] Gerace D, Andreani LC. Disorder-induced losses in photonic crystal waveguides with line defects. Opt Lett 2004;29:1897–99.
[42] Kuramochi E, Notomi M, Hughes S, Shinya A, Watanabe T, Ramunno L. Disorder-induced scattering loss of line-defect waveguides in photonic crystal slabs. Phys Rev B 2005;72:161318(R).
[43] Perez-Galacho D, Baudot C, Hirtzlin T, et al. Low voltage 25Gbps silicon Mach-Zehnder modulator in the O-band. Opt Express 2017;25:11217–22.
[44] Yong Z, Sacher WD, Huang Y, et al. U-shaped pn junctions for efficient silicon Mach-Zehnder and microring modulators in the O-band. Opt Express 2017;25:8425–39.
[45] Jin J. The finite element method in electromagnetics. New York: John Wiley & Sons, 2002.
[46] Maegami Y, Cong G, Ohno M, Okano M, Yamada K. Strip-loaded waveguide-based optical phase shifter for high-efficiency silicon optical modulators. Photon Res 2016;4:222–6.
[47] Hugonin JP, Lalanne P, Del Villar I, Matias IR. Fourier modal methods for modeling optical dielectric waveguides. Opt Quantum Electron 2005;37:107–19.
[48] Shi W, Xu Y, Sepehrian H, La Rochelle S, Rusch LA. Silicon photonic modulators for PAM transmissions. J Opt 2018;20:083002.